PHYSICAL REVIEW E **92**, 050902(R) (2015)

Recurrent noise-induced phase singularities in drifting patterns

M. G. Clerc,[1] S. Coulibaly,[2] F. del Campo,[1] M. A. Garcia-Nustes,[3] E. Louvergneaux,[2,*] and M. Wilson[2]

[1]*Departamento de Física, FCFM, Universidad de Chile, Casilla 487-3, Santiago, Chile*

[2]*Laboratoire de Physique des Lasers, Atomes et Molécules, CNRS UMR 8523, Université Lille1, 59655 Villeneuve d'Ascq Cedex, France*

[3]*Instituto de Física, Pontificia Universidad Católica de Valparaíso, Avenida Brasil, Valparaíso, Casilla 2950, Chile*

(Received 18 February 2014; revised manuscript received 29 July 2015; published 6 November 2015)

We show that the key ingredients for creating recurrent traveling spatial phase defects in drifting patterns are a noise-sustained structure regime together with the vicinity of a phase transition, that is, a spatial region where the control parameter lies close to the threshold for pattern formation. They both generate specific favorable initial conditions for local spatial gradients, phase, and/or amplitude. Predictions from the stochastic convective Ginzburg-Landau equation with real coefficients agree quite well with experiments carried out on a Kerr medium submitted to shifted optical feedback that evidence noise-induced traveling phase slips and vortex phase-singularities.

DOI: 10.1103/PhysRevE.92.050902 PACS number(s): 05.45.−a, 42.65.−k, 45.70.Qj

Nonequilibrium systems are characterized by their ability to exhibit self-organized structures or patterns as a result of the balance between energy injection and dissipation [1,2]. In the vicinity of phase transition, experimental observations and theoretical works report the emergence of traveling phase singularities [3–15], for instance, phase slip, which corresponds to a slippage of the phase [16]. This behavior of traveling spatial phase defects can be either transitory or permanent and are associated with amplitude holes. These topological defects play a fundamental role in transient phenomena [10,17] (like the evolution of the early Universe [18]) and are candidates to be the primary form of one-dimensional weak turbulence [19,20]. Thus, the study of phase defects is of primary importance in a better understanding of these objects.

The aim of this Rapid Communication is to show that the presence of noise near the primary threshold of spatial instability in drifting systems gives rise to recurrent creation of traveling phase singularities. We show that the emergence of such recurrent phase singularities implies specific initial conditions. The first condition is given by noise as a source for local spatial gradients and the second one by a spatial region where the control parameter lies close to the threshold for pattern formation (e.g., control parameter inhomogeneities or boundary conditions). A third one is of course a convective regime for the traveling of phase defects. Here, considering the stochastic drifting Ginzburg-Landau (GL) equation in the limit of real coefficients, we demonstrate that these three key ingredients allow us to generate recurrent traveling unstable phase slip (hole) solutions in one spatial dimension and topologically stable vortices for two spatial dimensions. Experiments on a Kerr medium with shifted optical feedback, which is modeled by the GL equation, confirm the creation of phase slip and vortex phase singularities in noise-sustained drifting patterns.

Since we are interested in the recurrent creation of traveling spatial phase defects, we will consider propagative patterns. They are generally induced by spatial inhomogeneities or gradient flows that create drift forces on these patterns. For high enough value of the drift strength, patterns can enter in the region of convective instability [21] where they first develop but vanish at long times. When the macroscopic system is subjected to inherent fluctuations, the convective regime is replaced by a noise-sustained structure regime [22–24], i.e., spatial structures that exclusively survive thanks to the presence of noise. This phenomenon was observed in several physical contexts such as nonlinear optics [21,25,26] and hydrodynamics [24].

Phase singularities in drifting patterns. To shed light on the mechanism of noise-induced phase singularities in drifting patterns, we consider the GL equation with real coefficients that describes the spatiotemporal evolution of the slowly varying envelope $A(x,t)$ close to the spatial bifurcation [2]. In the presence of noise and convection forces, the equation becomes the dimensionless stochastic and drifting Ginzburg-Landau equation [27]

$$\partial_t A = \mu A - |A|^2 A + i\beta A + \partial_{xx} A + c\partial_x A + \sqrt{\eta}\zeta', \quad (1)$$

where μ is the bifurcation parameter, c is the group velocity, and β stands for phase velocity. $\zeta'(x,t)$ represents a delta correlated white noise with intensity η. In the moving frame of reference $x' = x - ct$, Eq. (1) becomes a GL equation with real coefficients and without drift. However, in a finite system with boundary conditions, Eq. (1) remains propagative and drift plays an essential role in its dynamics.

Numerical simulations of Eq. (1) close to the primary convective instability threshold and imposing boundary conditions such that $A(x = 0,t)$ on the left and Neumann boundary condition on the right, show a noise-sustained drifting wave with a recurrent stochastic appearance of defects (Fig. 1). The envelope of the traveling wave shows that these defects are associated with localized holes in the drifting wave amplitude [Fig. 1(b)]. Figure 1(d) is a cross-section intensity profile of the spatiotemporal diagram Fig. 1(a). It evidences a propagating hole in the wave envelope profile. The corresponding pattern wave number profile [Figs. 1(e) and 1(c)] depicts a large excursion or deviation at the location of the amplitude hole, indicating a large phase gradient. The surrounding mean value of the local wave number on both

*eric.louvergneaux@univ-lille1.fr; http://www.phlam.univ-lille1.fr/spip.php?article66

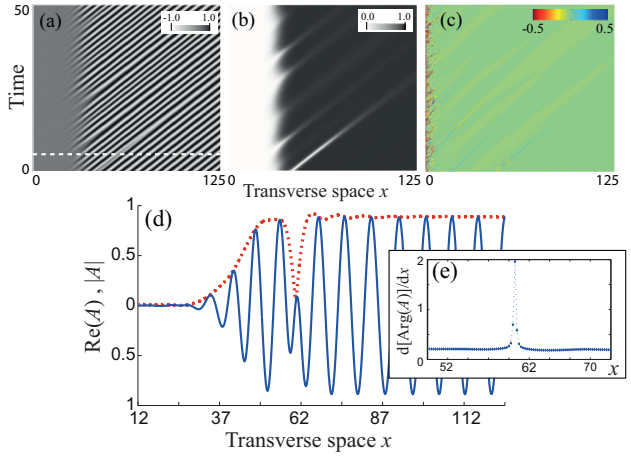

FIG. 1. (Color online) Spatiotemporal diagram of amplitude Eq. (1). (a) The real part of $A(x,t)e^{iqx}$, (b) $|A|$, (c) phase gradient (local wave number), and (d) a snapshot profile of the real part of $A(x,t)e^{\imath qx}$ (continuous curve) and the pattern amplitude $|A|$ (dashed curve) for time corresponding to the dashed line in (a). Parameters: $\mu = 0.2$, $\beta = 2.0$, $c = 3.0$, $q = 1.0$, $\eta = 4 \times 10^{-5}$, $dt = 0.03$, and $dx = 0.25$ with Dirichlet boundary on the left $[A(x = 0,t) = 0]$ and Neumann boundary condition on the right. (e) Phase gradient profile in the vicinity of the amplitude hole of (d). The numerical simulations were conducted using Runge-Kutta order 4 and finite element methods.

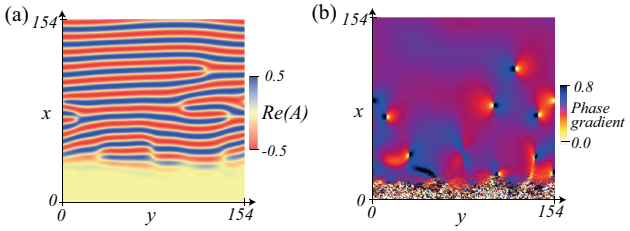

FIG. 2. (Color online) Noise-induced vortices of amplitude Eq. (3). The real part (a) and the phase gradient (b) of $A(\vec{r},t)e^{iqx}$, with $\mu = 0.7625$, $\beta = 1.875$, $c = 2.5$, $q = 0.75$, $\eta = 1 \times 10^{-8}$, $dt = 0.03$, and $dx = 0.3$. Zero boundary condition at $x = 0$ and Neumann boundary conditions elsewhere. Same integration methods as for Fig. 1.

sides of the hole are the same. The localized hole corresponds to fronts connecting two regions of a pattern whose wavelength is the same but the phase is different. During propagation, their dips continuously move away until they disappear. Such type of holes are known as a one-parameter family of homoclinic solutions of GL with real coefficients [16,20] and are expected to occur during the Eckhaus instability [28]. For a positive bifurcation parameter, the traveling hole solutions or phase slip of Eq. (1) is written as

$$A_{PS} = -\sqrt{\mu}\tanh\left(\sqrt{\frac{\mu}{2}}(x - ct)\right)e^{i[\beta t + \pi\Theta(x-ct)]}, \quad (2)$$

where $\Theta(x - ct)$ is the Heaviside function. The phase experiences a jump which is characterized by a Dirac function for its derivative (wave number; cf. Fig. 1). Straightforward, linear stability analysis proves that this solution is unstable. The hole rises and becomes flat as it propagates [20], leaving a fading trace.

In the system without noise, $\eta = 0$, spontaneous creation of holes may appear by the Eckhaus instability, but the recurrent feature of hole creation is lost. A requirement for such hole creation is related to particular conditions that must provide a local amplitude depression of the wave pattern [4] or a phase jump. In the stochastic case such requirement is given by the noise in the threshold vicinity, where the amplitude of the emerging pattern is small, the depletion region [10]. The recurrence feature is provided by the perpetual renewal of local spatial gradients imposed by the noise source term. Thus, the creation of a phase defect can occur through either bulk instability [28] or spatial inhomogeneity of one control parameter [29,30]; they can also appear following specific conditions that generate either a local amplitude depletion of the initial wave pattern or a local phase gradient. This is the mechanism of recurrent creation of phase singularities in our drifting system.

Let us consider now the amplitude equation in two spatial dimensions. Since all anisotropy stems from the dominant wave vector and from drift, we have

$$\partial_t A = \mu A - |A|^2 A + \imath\beta A + \nabla^2 A + c\partial_x A + \sqrt{\eta}\zeta'. \quad (3)$$

Here, phase singularities correspond to vortices, which are topologically stable [31]. They have a positive or negative charge depending on a $\pm 2\pi$ phase jump. Vortices are advected with the pattern until they disappear by annihilation with a vortex of opposite charge or through a boundary. The mechanism of creation is qualitatively the same as for the one-dimensional (1D) case; in the region of low amplitude, noise dominates dynamics and is able to turn both real and imaginary parts of the field to zero (Fig. 2). The deterministic mechanisms for the creation of defects as in the defect-mediated turbulence [19] or spatiotemporal intermittency [32] regimes do not apply in our case since the presented defects are only created in the region of the primary threshold for transverse instability.

Kerr feedback system. The experimental setup in which the noise-induced phase singularities are observed is composed by a thin liquid crystal cell (Kerr-like medium) subjected to optical tilted feedback (cf. Fig. 3). This configuration allows the generation of rich spatiotemporal dynamics [21]. Noise originates from thermal fluctuations that induce random motion of the molecular axis of the liquid crystal. 1D and two-dimensional (2D) transverse pumpings can be achieved with the help of a cylindrical lens telescope [34]. When the feedback mirror M is tilted with an angle 2α, the backward field B is transversely translated of a distance h with respect to the incoming field F. This nonlocal feedback makes the system convectively unstable with the emergence of drifting patterns [21,26].

The model governing the nonlinear refractive index perturbations $n(x,t)$ of the nematic liquid crystal around its uniform and stationary state $n_0 = F^2(1 + R)$ $(n \ll n_0)$ reads

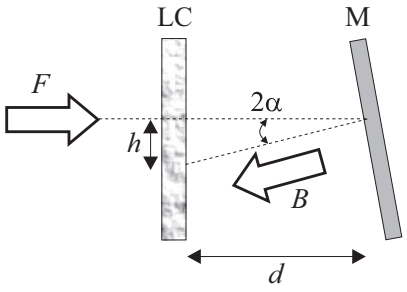

FIG. 3. Experimental scheme of the Kerr feedback system. A thin liquid crystal slice (LC) is submitted to an optical feedback via forward F and backward B fields. Technically, a 50-μm-thick layer of $E7$ homeotropically aligned nematic liquid crystal is irradiated by a 532 nm frequency doubled Nd:YVO4 laser. The typical diameter of the input beam is 3 mm and its linear polarization is perpendicular to its propagation, in the plane of the current sheet. A more detailed description of the setup can be found in [33].

[26,35,36]

$$\frac{\partial n}{\partial t} - \partial_{\perp}^2 n + n = I R\left(\left|e^{i\sigma\partial_{\perp}^2} e^{i\chi n(x+h,t)}\right|^2 - 1\right) + \sqrt{\eta}\zeta(x,t), \tag{4}$$

where $I = F^2$, t and $\mathbf{r} = (x,y)$ are the time and transverse space variables scaled with respect to the relaxation time τ and the diffusion length l_d; R is the mirror intensity reflectivity. We have set $\sigma = d/k_0 {l_d}^2$, where d is the slice-mirror distance and k_0 is the optical wave number of the field. $\zeta(\mathbf{r},t)$ accounts for thermal noise and describes a Gaussian stochastic process of zero mean value and correlation $\langle\zeta^*(\mathbf{r},t)\zeta(\mathbf{r}',t')\rangle = \delta(\mathbf{r}-\mathbf{r}')\delta(t-t')$, $\langle\zeta(\mathbf{r},t)\zeta(\mathbf{r}',t')\rangle = 0$. The level of noise is controlled by the parameter η. F is the forward input optical field; its transverse profile is accounted for using $F(\mathbf{r}) = F_0 g(\mathbf{r})$, with $g(\mathbf{r}) = \exp[-(x^2+y^2)/w^2]$ for a Gaussian pump beam of radius w and $g = 1$ for the uniform (plane wave) case. B is the backward optical field. The Kerr effect is parametrized by χ, which is positive (negative) for a focusing (defocusing) medium. Starting from the above model, in the plane wave approximation [$g(\mathbf{r}) = 1$], in absence of noise ($\eta = 0$), and assuming perturbations of the stationary state n_0 in the form $n(\mathbf{r},t) \sim A(\mathbf{r},t)\exp i[\mathbf{kr} - \Omega(\mathbf{k})t]$ with $\mathbf{k} = (k_x,k_y)$, the dispersion relation can be written as $\Omega = \Omega^r + i\Omega^i = -i[1 + \mathbf{k}^2 - \mu\,\sin(\sigma\mathbf{k}^2)\exp(ihk_x)]$. Transverse instability occurs above a critical instability threshold $I_c(k,h)$ given by $\Omega^i = 0$. The critical wave number k_c associated with the primary threshold for instability comes from the condition $\partial\Omega^i/\partial\Re(k) = 0$. Therefore, for intensities $I < I_c$, the homogeneous refractive index n_0 is stable. When $I > I_c$ the system is characterized by the emergence of traveling patterns.

To describe the emergence of patterns close to the spatial instability threshold, we use the method of weak nonlinear analysis, which is based on finding the amplitude equation, through a change of variables near the identity in power series of the critical amplitude [37–39], with stochastic terms [40,41]. We only present here the one-dimensional case. Considering series expansion for $\exp(i\chi n)$ and operator $e^{i\sigma\partial_{xx}^2}$ and considering the dominant terms ($h \ll \mathbf{k}$ and $n \ll 1$), Eq. (4) becomes

$$\begin{aligned}\frac{\partial n}{\partial t} - \partial_{xx}^2 n + n = RI\Big[&-2\chi\,\sin\left(\sigma\partial_{xx}^2\right)(n + h\partial_x n)\\ &-\chi^2\cos\left(\sigma\partial_{xx}^2\right)n^2 + \chi^2\left[\sin\left(\sigma\partial_{xx}^2\right)n\right]^2\\ &+\chi^2\left[\cos\left(\sigma\partial_{xx}^2\right)n\right]^2 + \frac{\chi^3}{3}\sin\left(\sigma\partial_{xx}^2\right)n^3\\ &+\chi^3\cos\left(\sigma\partial_{xx}^2\right)n^2\sin\left(\sigma\partial_{xx}^2\right)n\\ &-\chi^3\cos\left(\sigma\partial_{xx}^2\right)n\,\sin\left(\sigma\partial_{xx}^2\right)n^2\\ &+h.o.t. + \sqrt{\eta}\zeta(x,t)\Big].\end{aligned} \tag{5}$$

Because this nonlocal equation now explicitly has powers in the effective index of refraction $n(x,t)$, one can then perform the weakly nonlinear analysis [37–40]. Introducing the bifurcation parameter $\epsilon \equiv (I - I_c)/I_c$ and using the ansatz $n(x,t) = C(y,t)e^{ik_c x} + a_1 C^2 e^{2ik_c x} + W + \text{c.c.}$ where $C \equiv C(y,t)$ is the slowly varying complex amplitude of the pattern envelope, with $y = \sqrt{\epsilon}x$ as the spatial slow variable, x the fast one, $a_1 \equiv RI\chi^2[1 - \cos(4\sigma k_c^2)]/[1 + 4k_c^2 - 2RI\chi\,\sin(\sigma k_c^2)]$, and $W \equiv W(C(x,t),x)$ is a small correction function of order $\mu^{3/2}$, which expresses itself as a power series in the amplitude C ($W \ll C^2$, $C \ll 1$, $\partial_t C \ll C$, and $\partial_{yy}C \ll \partial_y C$). Introducing the above ansatz in Eq. (5) and linearizing in W, after straightforward calculation, we find

$$\partial_t A = \mu A - |A|^2 A + i\beta A + c\partial_X A + \partial_{XX}A + \sqrt{\eta}\xi, \tag{6}$$

where $A(X,t) = C\,e^{i\alpha X/2}\sqrt{\rho}$, $\mu = 2\epsilon R\chi\,\sin(\sigma k_c^2) - \beta^2$, $\beta = 2RI_c\chi k_c h\,\sin(\sigma k_c^2)$, $c = 2RI_c\chi k_c h\,\cos(\sigma k_c^2)$, $X = x/\sqrt{d}$, $\xi = (k_c/2\pi)\int_x^{x+2\pi/k_c}\zeta(x',t)e^{-ik_c x'}dx'$, and $\rho = RI_c\chi^2\{3\chi\,\sin(\sigma k_c^2) - \chi\,\sin(3\sigma k_c^2) + 2a_1\chi[\cos(\sigma k_c^2) - \cos(3\sigma k_c^2)]\}$. Therefore, we recover Eq. (1), where the parameters of the amplitude equation are directly related to the parameters of the Kerr medium submitted to shifted optical feedback. Note that the bifurcation parameter is the intensity of the input beam (I). The group and phase velocity are related to the lateral shift (h).

Experimental traveling holes. When the system is pumped with a quasi-1D transverse laser beam and the feedback mirror is tilted by approximately 1.5 mrad, a line of drifting spots induced by noise is observed [26]. Its spatiotemporal profile intensity evolution is depicted in Fig. 4(a) for a pumping value in the vicinity of the primary instability threshold. In this situation, the system shows defect lines that always accompany the spatiotemporal diagrams, as pointed out by the arrows in Fig. 4(a).

The spatial local phase and envelope of the pattern, extracted from the signal constructed with the help of Hilbert transformation [43,44], are reported in Figs. 4(b) and 4(d) for the amplitude and the phase, respectively. The pattern envelope [Fig. 4(b)] clearly evidences traveling-hole lines corresponding to amplitude holes as plotted in Fig. 4(e). Corresponding Fig. 4(d) shows that these amplitude holes are associated with phase defects whose gradient varies rapidly [Fig. 4(c)]. A cross section of the pattern modulation [Fig. 4(e)] taken from Fig. 4(a) depicts such a typical envelope hole with zero amplitude. The wave number deforms itself to follow the

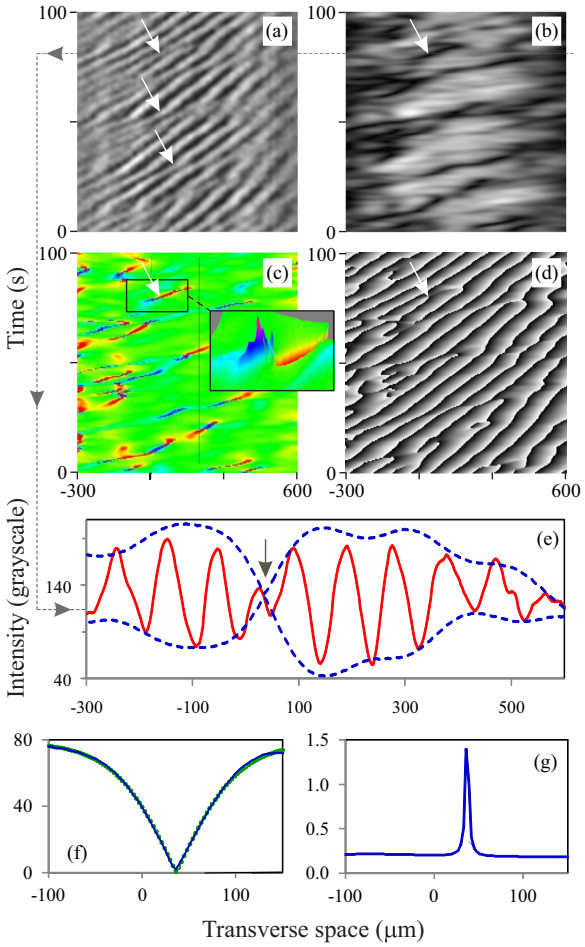

FIG. 4. (Color online) (a) Spatiotemporal evolution of the experimental transverse intensity of the output beam B_{out} for the 1D transverse pumping configuration. (b)–(d) are its corresponding pattern (b) envelope, (c) wave number (or phase gradient), and (d) phase, respectively. (c) The black frame in the wave number spatiotemporal diagram locates a hole solution whose profile is reported on (f); its related 3D wave number view is given in the translated close-up frame. (e) Pattern modulation (continuous red line) and envelope outline [42] (dashed blue line) cross sections taken from (a) and (b) at times equal to 80 s. (f) Close-up of the amplitude hole (green dots) indicated by the arrow at $x = 36$ μm on (e) together with the best fit using traveling hole solution, Eq. (2) (continuous curve). (g) Wave number variation in the vicinity of the hole located at $x = 36$ μm. $d = 5$ mm, $h = 13$ μm, and $\alpha = 1.3$ mrad.

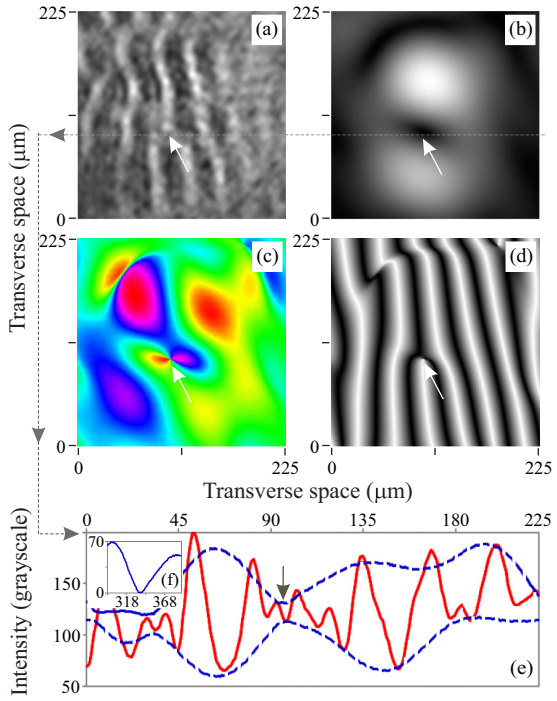

FIG. 5. (Color online) (a) Snapshot of the transverse intensity pattern of the output beam B_{out} for the 2D transverse pumping configuration. (b)–(d) are its corresponding pattern (b) envelope, (c) phase gradient (or wave number), and (d) phase, respectively. (e) Pattern modulation (continuous red line) and envelope outline [42] (dashed blue line) cross sections taken from (a) and (b) at position $y = 105$ μm. (f) Close-up of the amplitude hole indicated by the arrow on (e). The vortex corresponds to the defect in the vertical roll structure (a) that travels to the left. $d = 5$ mm, $h = 90$ μm, and $\alpha = 9$ mrad.

hole phase jump, with a very fast spatial variation [Fig. 4(g)] in good agreement with Eq. (2). Let us mention that this fast local change is inverted, following the evolution path of a hole, from before to after the creation of a zero amplitude hole. This can be seen on the three-dimensional (3D) frame of Fig. 4(c) where the local wave number variation is positive for time before 80 s (mountain shape) and negative afterwards (canyon shape). This is always the case when a hole with zero amplitude is created. The fit [continuous line in Fig. 4(f)] of such an experimental zero-amplitude hole (dots) by the analytical hole solution, Eq. (2), gives a relative rms of residuals [45] of 8.8×10^{-3}.

Hence, the result of this regression together with the previous features are good arguments for the evidence of phase slip in our experimental setup. These hole states are induced by noise at the onset of pattern formation [10]. Since the depicted transverse domain of Fig. 4 is 900 μm wide and the Gaussian beam diameter is 3000 μm, the transverse pumping parameter varies less than 10% with respect to its maximum value. This means that almost the whole depicted transverse domain belongs to the threshold vicinity region. Thus, the region where the phase defects are most likely to develop is left [$x_0 \approx -300$ μm in Figs. 4(a)–4(d)] but the rest of the domain is also favorable to the appearance of such structures. Indeed, holes appear randomly and repeatedly with time mostly in the vicinity of x_0 due to thermal fluctuations, but from time to time also in the rest of the transverse domain. They have a life duration that strongly varies depending on the phase defect annihilation mechanism and the escape from the threshold boundaries. They drift with a mean group velocity $V_h \simeq 53 \pm 3.5$ μm/s (whereas the modulational instability phase velocity is $V_{MI} = 12 \pm 0.8$ μm). Their trajectories display leaps (undulations) as observed in the pinning-depinning phenomenon induced by the Gaussian profile inhomogeneities in the same system [27]. Numerical simulations carried out on the deterministic model, Eq. (4), associated with the current

experiments, evidence unstable holes [the fit using expression (2) gives a relative rms of residuals [45] equal to 14.3×10^{-3}], but only for very specific initial conditions close to hole solution (2). That is, numerical simulations carried out with other initial conditions never depict such amplitude holes. On the contrary, stochastic simulations, at the onset of spatial bifurcation, clearly show recurrent creation of holes with time thanks to noise that randomly generates local conditions for the real and imaginary parts of the optical field close to phase singularity, Eq. (2). Thus, noise acts as a source term for phase defect generation in the vicinity of the phase transition from the homogeneous state to the modulational unstable one. Moreover, thanks to the combined effect of the drift and the vicinity of the pumping parameter threshold for pattern formation, these amplitude holes are repeatedly emitted with time.

Noise-sustained vortices. For the 2D transverse laser beam pumping configuration, a drifting vertical roll pattern [Fig. 5(a)], at $h = 90$ μm, replaces the standard hexagonal lattice obtained for the case without any translational shift ($h = 0$). As for the 1D configuration, holes appear randomly and repeatedly with time. Such a defect in the roll structure, looking like a dislocation defect, is pointed out by an arrow in Fig. 5(a). This defect travels to the left with time in the transverse cross section of the system as propagating amplitude holes in the previous 1D configuration. To identify the nature of this propagating defect, we follow the same procedure as previously to extract pattern amplitude and phase. The results of the pattern processing is reported in Fig. 5. Figure 5(d) evidences the existence of a 2D phase defect associated with a corresponding local zero roll modulation amplitude value as can be checked on the transverse profile [Fig. 5(e)] of the roll envelope [Fig. 5(b)]. The associated local variation of the phase gradient also depicts a discontinuity [Fig. 5(c)]. All these properties indicate that the roll pattern defect is a vortex. It is stable and induced as previously by the noise.

In summary, we have shown that perpetual emission of phase singularities, can be readily produced and observed in noisy convective systems in the vicinity of the threshold for pattern formation. In this transition regime, local spatial inhomogeneities can initiate phase defects. The combined role of the drift, the vicinity of a transition, and noise then generates the favorable initial conditions for the recurrent generation of such phase singularities. We have thus evidenced the creation of unstable phase slip and topologically stable vortices in one and two spatial dimensions, respectively. Hence, the GL equation with real coefficients is well suited as an amplitude equation for the pattern dynamics of our experimental system. These optic results generalize the existence of noise-induced phase singularities in drifting systems.

Acknowledgments. We acknowledge financial support of the ANR international program, project ANR-2010-INTB-402-02 (ANR-CONICYT 39). M.G.C., M.A.G.N., and M.W. acknowledge the financial support of FONDECYT 1150507, 11130450, and 3140387, respectively. F.d.C. acknowledges the financial support of CONICYT by *Beca Magister Nacional.* This research was also supported in part by the *Conseil Régional Nord-Pas de Calais*, *The Fonds Européen de Développement Economique des Régions.*

[1] G. Nicolis and I. Prigogine, *Self-Organization in Nonequilibrium Systems* (Wiley, New York, 1977).
[2] M. C. Cross and P. C. Hohenberg, Rev. Mod. Phys. **65**, 851 (1993).
[3] K. Nozaki and N. Bekki, J. Phys. Soc. Jpn. **53**, 1581 (1984).
[4] J. Lega, B. Janiaud, S. Jucquois, and V. Croquette, Phys. Rev. A **45**, 5596 (1992).
[5] S. Popp, O. Stiller, I. Aranson, and L. Kramer, Phys. D Nonlinear Phenom. **84**, 398 (1995).
[6] F. S. Roux, J. Opt. Soc. Am. B **12**, 1215 (1995).
[7] Y. Kivshar, J. Christou, V. Tikhonenko, B. Luther-Davies, and L. M. Pismen, Opt. Commun. **152**, 198 (1998).
[8] U. Morgner and F. Mitschke, Phys. Rev. E **58**, 187 (1998).
[9] J. Burguete, H. Chaté, F. Daviaud, and N. Mukolobwiez, Phys. Rev. Lett. **82**, 3252 (1999).
[10] S. Ducci, P. Ramazza, W. González-Viñas, and F. Arecchi, Phys. Rev. Lett. **83**, 5210 (1999).
[11] L. Pastur, M. Westra, and W. V. D. Water, Phys. D Nonlinear Phenom. **174**, 71 (2003).
[12] D. Amroun-Aliane, L. Pastur, and C. Letellier, Phys. Rev. E **83**, 056212 (2011).
[13] A. Chabchoub, O. Kimmoun, H. Branger, N. Hoffmann, D. Proment, M. Onorato, and N. Akhmediev, Phys. Rev. Lett. **110**, 124101 (2013).
[14] M. van Hecke, Phys. Rev. Lett. **80**, 1896 (1998).
[15] N. Bekki and K. Nozaki, Phys. Lett. **110**, 133 (1985).
[16] J. S. Langer and V. Ambegaokar, Phys. Rev. **164**, 498 (1967).
[17] P. C. Hendry, N. S. Lawson, R. A. M. Lee, P. V. E. McClintock, and C. D. H. Williams, Nature (London) **368**, 315 (1994).
[18] T. Kibble, Phys. Rep. **67**, 183 (1980).
[19] P. Coullet, L. Gil, and J. Lega, Phys. Rev. Lett **62**, 1619 (1989).
[20] J. Lega, Phys. D (Amsterdam, Neth.) **152-153**, 269 (2001).
[21] G. Agez, P. Glorieux, M. Taki, and E. Louvergneaux, Phys. Rev. A **74**, 043814 (2006).
[22] R. J. Deissler, J. Stat. Phys. **40**, 371 (1985).
[23] R. Deissler, J. Stat. Phys. **54**, 1459 (1989).
[24] J. García-Ojalvo and J. M. Sancho, *Noise in Spatially Extended Systems* (Springer, New York, 1999).
[25] M. Santagiustina, P. Colet, M. San Miguel, and D. Walgraef, Phys. Rev. Lett. **79**, 3633 (1997).
[26] E. Louvergneaux, C. Szwaj, G. Agez, P. Glorieux, and M. Taki, Phys. Rev. Lett. **92**, 043901 (2004).
[27] M. G. Clerc, C. Fernandez-Oto, M. A. García-Ñustes, and E. Louvergneaux, Phys. Rev. Lett. **109**, 104101 (2012).
[28] L. Kramer and W. Zimmermann, Phys. D (Amsterdam, Neth.) **16**, 221 (1985).
[29] H. Riecke and H. Paap, Phys. Rev. Lett. **59**, 2570 (1987).
[30] H. Riecke and H.-G. Paap, Europhys. Lett. **14**, 433 (2007).
[31] L. M. Pismen, *Patterns and Interfaces in Dissipative Dynamics*, Springer Series in Synergetics (Springer, Berlin/Heidelberg, 2006).
[32] H. Chate, Nonlinearity **7**, 185 (1994).

[33] G. Agez, C. Szwaj, E. Louvergneaux, and P. Glorieux, Phys. Rev. A **66**, 063805 (2002).

[34] E. Louvergneaux, V. Odent, M. I. Kolobov, and M. Taki, Phys. Rev. A **87**, 063802 (2013).

[35] S. Akhmanov, M. Vorontsov, and V. Y. Ivanov, JETP Lett. **47**, 707 (1988).

[36] W. J. Firth, J. Mod. Opt. **37**, 151 (1990).

[37] C. Elphick, E. Tirapegui, M. Brachet, P. Coullet, and G. Iooss, Physica D **29**, 95 (1987).

[38] G. Iooss and M. Adelmeyer, *Topics in Bifurcation Theory and Applications* (World Scientific, Singapore, 1998).

[39] A. Newell, T. Passot, and J. Lega, Annu. Rev. Fluid Mech. **25**, 399 (1993).

[40] E. Tirapegui, *Lecture Notes in Mathematics*, edited by R. Bamón, R. Labarca, and J. Palis, Jr. (Springer Verlag, Berlin, 1986), Vol. 1331.

[41] M. Clerc, C. Falcón, and E. Tirapegui, Phys. Rev. E **74**, 011303 (2006).

[42] The lower and upper amplitude envelope are plotted by subtracting or adding the amplitude obtained from the Hilbert transform to the dc field component.

[43] B. Boashash, Proc. IEEE **80**, 520 (1992).

[44] We first extract the transverse profile of the instability modulation amplitude using an Hilbert band pass filtering around the critical wave number. Then, we extract the unmodulated profile using a low pass filtering. The differences between them give the upper and lower envelopes of the pattern modulation.

[45] The relative rms of residuals is defined as the ratio between the rms of residuals to the hole amplitude. The rms comes from the fit using GNUPLOT software (http://gnuplot.sourceforge.net/). It corresponds to the square root of the final sum of squares of residuals to the degrees of freedom.